Lunar response to gravitational waves

M. Kachelrieß and M. P. Nødtvedt
Institutt for fysikk, NTNU, Trondheim, Norway

(Received 2 January 2024; accepted 8 August 2024; published 10 September 2024)

It has been suggested to use seismic detectors on the Moon as a tool to search for gravitational waves in an intermediate frequency range between mHz and Hz. Employing three different spherically symmetric models for the lunar interior, we investigate the response of the Moon to gravitational waves in Einstein and Jordan-Brans-Dicke gravity. We find that the first eigenfrequencies of the different models depend only weakly on the model details, with the fundamental frequency ν_1 close to 1 ms both for spheroidal and toroidal oscillations. In contrast, the resulting displacement varies up to a factor 5, being in the range $(3.6 \times 10^{12}\text{–}1.9 \times 10^{13})/h_0$ cm for spheroidal oscillations with amplitude h_0 and assuming a quality factor $Q_n = 3300$. Toroidal oscillations are suppressed by a factor $2\pi\nu R/c$, both in Einstein gravity and in general scalar-tensor theories.

DOI: 10.1103/PhysRevD.110.064034

I. INTRODUCTION

Historically, the excitation of vibrational eigenmodes in an elastic body was one of the first signatures suggested as proof for the existence of gravitational waves (GWs). In addition to the use of resonant bars on the laboratory scale, Weber also pointed out that GWs could be searched for monitoring the vibrations of the Earth or Moon [1]. The first calculation of the response of the Earth to a GW was performed soon later by Dyson, assuming a flat homogeneous Earth model [2]. The response of the Earth to a GW for a spherically, heterogeneous Earth model was first determined by Ben-Menahem [3], who followed the approach developed by Alterman *et al.* [4] for the study of seismic waves in the Earth.

Searches for GW using seismographs on Earth started already in the 1970s [5,6]. More recently, seismic data were used to derive stringent limits on the stochastic GW background in the frequency range 0.05–1 Hz [7]. In Ref. [8], the response of a nonrotating anelastic Earth model to a GW was revisited. On the Moon, the Lunar Surface Gravimeter experiment was deployed by Apollo 17, but technical problems prevented the usage of its data. In the last few years, the idea to use the Moon as GW detector has been revived and several new concepts were proposed: One type of experiments proposes constructing long-baseline interferometers similar to the successful LIGO setup, as e.g., the LION proposal [9] or the Gravitational-Wave Lunar Observatory for Cosmology GLOC [10]. Another type of proposal aims to exploit the response of the Moon to GWs similar to the original Weber suggestion, as, e.g., the Lunar Gravitational-Wave Antenna (LGWA) experiment [11] or the Lunar Seismic and Gravitational-Wave Antenna [12]. These lunar GW experiments could become an important partner observatory for joint observations with the space-borne, laser-interferometric detector LISA [13] and the planned underground Einstein observatory [14], exploiting the weak seismic activity of the Moon [15]. In particular, they could complement these observatories in the mHz range where their sensitivity has been estimated to be superior [11]. For instance, GWs from binary white-dwarf systems could be searched for by matching the frequencies of Moon's normal modes with the waveforms expected for these binaries [16]. For such searches, a precise understanding of the response of the Moon to GWs is a prerequisite.

In this work, we study the response of the Moon to gravitational perturbations employing and extending the approach of Ref. [3]. We derive a set of first-order differential equations which determine the eigenfunctions and eigenfrequencies of the Moon coupled to a GW for a given spherically, heterogeneous Moon model. We account for a potentially scalar polarization state in the GW, so that our results are also valid for general scalar-tensor theories of gravity like, e.g., Jordan-Brans-Dicke theories [17,18]. We determine the displacement and the eigenfrequencies of the first eigenmodes numerically for a set of three different Moon models. We find that there is very good agreement on the eigenfrequencies in all three models, while the magnitude of the displacement varies up to factor 2. Using the predicted capability to measure ground displacement in the LGWA experiment from Ref. [19], we find a nominal sensitivity to GWs with amplitude $h \simeq 10^{-20}$ in the mHz range assuming as quality factors $Q_n \simeq 3300$.

This work is structured as follows. In Sec. II, we recall the response of an elastic body to a GW in a general metric theory of gravity. We derive in Sec. III the normal modes of the Moon and summarize how its eigenfrequencies and displacements can be numerically calculated; most

technical details of this derivation are deferred into two Appendixes. Section IV introduces the models used to describe the Moon and presents our numerical results. Finally, we make concluding remarks in Sec. V.

II. RESPONSE OF AN ELASTIC BODY TO A GW

An elastic isotropic body with density ρ can be described in the nonrelativistic limit by the Lagrange density

$$\mathscr{L} = \frac{1}{2}\rho \dot{u}_i \dot{u}^i - \frac{1}{2}\varepsilon_{ij}\sigma^{ij}, \tag{1}$$

where u^i denotes the displacement of a body element. Its strain tensor ε_{ij} and stress tensor σ_{ij} are connected by the Cauchy relation,

$$\sigma_{ij} = \lambda\delta_{ij}\nabla_k u_k + \mu(\nabla_i u_j + \nabla_j u_i) = \lambda\delta_{ij}\nabla_k u_k + 2\mu\varepsilon_{ij}. \tag{2}$$

Both tensors depend on the two Lamé parameters λ and μ which determine the response of the body to bulk and shear forces.

The coupling of matter to an external gravitational perturbation $h_{\mu\nu}$ is at lowest-order perturbation theory given by $\mathscr{L}_{\rm int} = \kappa T_{\mu\nu}h^{\mu\nu}$ with $T_{\mu\nu}$ as the (relativistic) stress energy-momentum tensor and $\kappa = 8\pi G_N$ as the gravitational coupling. In the following, we do not impose the transverse-traceless (TT) gauge condition on $h^{\mu\nu}$. Instead, we assume only that gravitational waves (GW) satisfy $h_{0\mu} = h_{\mu 0} = 0$. Thus, we allow in particular for the possible presence of a scalar polarization state which might arise in theories of modified gravity. Then, the Lagrange density describing the elastic body under the influence of a GW is given by

$$\mathscr{L} = \mathscr{L}_0 + \mathscr{L}_{\rm int} = \frac{1}{2}\rho \dot{u}_i \dot{u}^i - \frac{1}{2}(\varepsilon_{ij} + h_{ij})\sigma^{ij}. \tag{3}$$

Thus, the GW acts, as expected, as an additional strain on the body. The equation of motion of the body follows as

$$\partial_t(\rho u^i) = \nabla_j\sigma^{ij} - \nabla_j(\mu h^{ij}) - \frac{1}{2}\nabla^i(\lambda h). \tag{4}$$

The last two terms represent the driving force density f_i exerted by the GW on the body,

$$f_i = -\nabla_j(\mu h_i{}^j) - \frac{1}{2}\nabla_i(\lambda h). \tag{5}$$

In Einstein gravity, where $h \equiv h_i{}^i = 0$ is valid in a physical gauge, the last term is absent. The corresponding stress is given by

$$\sigma_{ij} = -\mu h_{ij} - \frac{1}{2}\lambda h\delta_{ij}. \tag{6}$$

The GW in Eq. (4) can be represented as a superposition of monochromatic polarization states,

$$h_{ij}(t) = g(t)h_0\mathcal{E}_{ij}\sin(\omega t), \tag{7}$$

with amplitude h_0 and a time-dependent modulation given by $0 \le g(t) \le 1$. The polarization tensor $\mathcal{E}_{ij}$ contains in a general scalar-vector-tensor theory of gravity six independent components, $A_S, A_L, A_{V_1}, A_{V_2}, A_+$, and $A_\times$; see for an extended discussion, e.g., Ref. [20]. If the GW travels in the z direction, the polarization tensor has the form

$$\mathcal{E}_{ij} = \begin{bmatrix} A_S + A_+ & A_\times & A_{V_1} \\ A_\times & A_S - A_+ & A_{V_2} \\ A_{V_1} & A_{V_2} & A_L \end{bmatrix}. \tag{8}$$

In addition to the two polarization states A_+ and $A_\times$ present in Einstein gravity, two transverse (A_{V_1}, A_{V_2}) and one longitudinal A_L vector components as well as the scalar component A_s may enter $\mathcal{E}_{ij}$. As scalar extensions of Einstein gravity are far more popular than vector ones, we will neglect for simplicity the vector components in the following.

III. NORMAL MODES OF A SPHERICAL SELF-GRAVITATING BODY

A. Normal modes of a spherical body

The perturbations of a spherically symmetric body factorize in the variables t, r, and ϑ, ϕ. They are characterized by a set of eigenfunctions and eigenfrequencies which are specified by the three "quantum numbers" $\{n, m, l\}$. In a spherically symmetric body, the modes are degenerate in m. Neglecting for the moment the time dependence, the displacement vector for a given mode $\{n, m, l\}$ can be written as a linear combination of the three Hansen vectors, or equivalently as a sum of the vector surface harmonics $\boldsymbol{C}^{(ml)}, \boldsymbol{P}^{(ml)}$, and $\boldsymbol{B}^{(ml)}$,

$$\begin{aligned}\boldsymbol{u}(\boldsymbol{r}) = {} & U^{(n)}(r)\boldsymbol{P}^{(ml)}(\vartheta,\phi) + V^{(n)}(r)\sqrt{l(l+1)}\boldsymbol{B}^{(ml)}(\vartheta,\phi) \\ & + W^{(n)}(r)\sqrt{l(l+1)}\boldsymbol{C}^{(ml)}(\vartheta,\phi).\end{aligned} \tag{9}$$

In spherical coordinates, the vector surface harmonics are given by

$$\sqrt{l(l+1)}C_i^{(ml)}(\vartheta,\phi) = \left(\hat{e}_i^{(\vartheta)}\frac{1}{\sin\vartheta}\frac{\partial}{\partial\phi} - \hat{e}_i^{(\phi)}\frac{\partial}{\partial\vartheta}\right)Y^{(ml)}, \tag{10a}$$

$$P_i^{(ml)}(\vartheta,\phi) = \hat{e}_i^{(r)}Y^{(ml)}(\vartheta,\phi), \tag{10b}$$

$$\sqrt{l(l+1)}B_i^{(ml)}(\vartheta,\phi) = \varepsilon_{ijk}\hat{e}_j^{(r)}C_k^{(ml)}, \tag{10c}$$

where $\hat{\boldsymbol{e}}^{(j)} = \{\hat{\boldsymbol{e}}^{(r)}, \hat{\boldsymbol{e}}^{(\phi)}, \hat{\boldsymbol{e}}^{(\vartheta)}\}$ are orthonormal unit base vectors, ε_{ijk} denotes the Levi-Civita symbol, $P^{(ml)}(\vartheta, \phi)$ is the associated Legendre polynomial, and the spherical harmonics $Y^{(ml)}(\vartheta, \phi)$ are defined in Eq. (B5). In order to distinguish the indices labeling eigenmodes from coordinate indices, we set the former in parentheses. Since we use unit base vectors, we do not need to distinguish between upper and lower indices.

The eigenmodes can be split into two independent sets of modes: spheroidal oscillations (with $W^{(n)} = 0$) which modify the shape of the body and toroidal oscillations (with $U^{(n)} = V^{(n)} = 0$) which do not.

The time dependence of small oscillations $\boldsymbol{u}(\boldsymbol{r}, t) = \boldsymbol{u}(\boldsymbol{r})\bar{g}(t)$ of an elastic body are naturally modeled as a damped harmonic oscillator. Thus, the time-dependent effect of a monochromatic GW with frequency ω_0 on a elastic body follows as a Fourier integral of the Green's function $G_n(\omega)$ of a forced damped harmonic oscillator with eigenfrequency ω_n weighted by $g(\omega)$,

$$\bar{g}_n(t) = \int \frac{\mathrm{d}\omega}{2\pi} g(\omega) \mathrm{e}^{\mathrm{i}\omega_0 t} G_n(\omega) \tag{11a}$$

$$= \int \frac{\mathrm{d}\omega}{2\pi} \frac{g(\omega)\mathrm{e}^{\mathrm{i}\omega_0 t}}{\omega_n^2 - \omega^2 + \mathrm{i}\omega_n \omega / Q_n}. \tag{11b}$$

Here, $g(\omega)$ is the Fourier transform of $g(t)$, while Q_n is the damping (or quality) factor of the mode n. Note that other choices for the Green's function are in use, which should differ mainly in how anharmonic terms in the response to the GW are parametrized. Our default choice of a forced damped harmonic oscillator is the one often employed in seismology, but we will present later results also for another Green's function.

As a simple model for $g(t)$, we consider for illustration a finite monochromatic GW of duration 2τ,

$$g(t) = [\vartheta(t+\tau) - \vartheta(t-\tau)]\mathrm{e}^{\mathrm{i}\omega_0 t}, \tag{12}$$

with $\vartheta(t)$ as the Heaviside step function. Then, $\bar{g}_n(t)$ follows as

$$\bar{g}_n(t) \simeq \frac{g(t)}{(\omega_0 - \omega_n)^2 + \omega_n^2/(4Q_n)} \tag{13}$$

in the limit $Q_n \gg 1$.

B. Linearization of Euler and Poisson equations

In Fourier space, the Euler equation becomes in spherical coordinates

$$\frac{\partial}{\partial r}\sigma_{ir} + \frac{1}{r}\frac{\partial}{\partial \vartheta}\sigma_{i\vartheta} + \frac{1}{r\sin\vartheta}\frac{\partial}{\partial \phi}\sigma_{i\phi} + \rho F_i + \rho\omega^2 u_i = 0. \tag{14}$$

We simplify this equation using the following assumptions: First of all, we restrict ourselves to linear perturbations. Then, we assume that the self-gravitating body is initially in equilibrium between the hydrostatic pressure gradient $\boldsymbol{\nabla} P^{(0)}$ and internal gravitational forces, $\boldsymbol{F}^{(0)} = \boldsymbol{f}^{(0)}/\rho = \boldsymbol{\nabla}\Psi^{(0)}$. Here, we introduced the gravitational (anti)potential $\Psi^{(0)}$, and we denote unperturbed quantities with the subscript zero. Being strained, a volume element carries its initial stress $\sigma^{(0)}(\boldsymbol{r}^{(0)})$ to its new position $\boldsymbol{r}^{(0)} + \boldsymbol{u}$. Thus,

$$\sigma_{ij}^{(0)}(\boldsymbol{r}^{(0)}) = \sigma_{ij}^{(0)}(\boldsymbol{r} - \boldsymbol{u}) = -P^{(0)}(\boldsymbol{r} - \boldsymbol{u})\delta_{ij}(\boldsymbol{r}) \tag{15a}$$

$$= -P^{(0)}(\boldsymbol{r}) - \boldsymbol{u}(\boldsymbol{r})\boldsymbol{\nabla}P^{(0)}(\boldsymbol{r})\delta_{ij}(\boldsymbol{r}) \tag{15b}$$

$$= -(P^{(0)} + g^{(0)}\rho^{(0)}u_r)\delta_{ij}(\boldsymbol{r}), \tag{15c}$$

where $g^{(0)}$ is the unperturbed gravitational acceleration. In addition, the volume element acquires an additional stress $\delta\sigma_{ij}$ after displacement due to distortions, given by the usual Cauchy relation. Thus,

$$\delta\sigma_{ij} = \lambda\delta_{ij}\nabla_k u_k + 2\mu\varepsilon_{ij}. \tag{16}$$

We can now insert the total stress $\sigma_{ij} = \sigma_{ij}^{(0)} + \delta\sigma_{ij}$ into Eq. (14). The divergence of the initial stress becomes

$$\nabla_k(\sigma_{ik}^{(0)}) = -\nabla_k(P^{(0)} + g^{(0)}\rho^{(0)}u_r)$$
$$= g^{(0)}\rho^{(0)}\hat{e}_k^r - \frac{\mathrm{d}\rho^{(0)}}{\mathrm{d}r}g^{(0)}u_r - \rho^0\nabla_k(g^0 u_r), \tag{17}$$

while the force term can be written as

$$\rho F_k = \left(\rho^{(0)} - \frac{\mathrm{d}\rho^0}{\mathrm{d}r}u_r - \rho^{(0)}\nabla_i u_i\right)(\nabla_k\psi - g^{(0)}\hat{e}_k^r)$$
$$= \rho^{(0)}\nabla_k\psi + g^{(0)}\left(\frac{\mathrm{d}\rho^{(0)}}{\mathrm{d}r}u_r + \rho^{(0)}\nabla_k u_k - \rho^{(0)}\right)\hat{e}_j^r, \tag{18}$$

where the continuity equation $\rho - \rho^{(0)} = \boldsymbol{\nabla}\cdot(\rho^{(0)}\boldsymbol{u})$ was used in the first step to expand ρ. Including the remaining part of Eq. (14), we arrive at the following differential equation

$$\nabla_k(\lambda\nabla_i u_i) + \mu[\Delta u_k + \nabla_k(\nabla_i u_i)]$$
$$+ \frac{\mathrm{d}\mu}{\mathrm{d}r}\left(2\frac{\partial u_k}{\partial r} + [\hat{e}^{(r)} \times (\nabla \times \mathbf{u})]_k\right)$$
$$+ \rho^{(0)}\nabla_k(\psi - g^{(0)}u_r) + \rho^{(0)}\hat{e}_k^{(r)}\nabla_i u_i + \omega^2\rho^{(0)}u_k = 0. \tag{19}$$

In addition, the potential $\Psi = \Psi^{(0)} + \psi$ obeys the Poisson equation, implying for the perturbation

$$\Delta\psi = -4\pi G(\rho - \rho^{(0)}) = 4\pi G\nabla_j(\rho^{(0)}u_j). \tag{20}$$

Equations (19) and (20) are the two coupled differential equations which we have to solve numerically under appropriate boundary conditions. We assume that the Moon, similar to the Earth, can be divided into a liquid core and a solid mantle. In this case, one can follow the procedure developed for the study of seismic waves in the Earth, as described in detail, e.g., in Ref. [21]. For the convenience of the reader, the transformation of Eqs. (19) and (20) to a set of linear differential equation for $\{y_1, \ldots, y_6\}$ is summarized in Appendix A.

C. Normal modes of a spherical self-gravitating body

As a consequence of our linearization, the Fourier modes $\{nml\}$ decouple, and we can consider the evolution of a single mode. Moreover, our assumption of spherical symmetry implies that the Euler and Poisson equations reduce to ordinary differential equation in the radial coordinate, while the angular dependence can be expressed as Fourier transforms of the vector surface harmonics on S^2, which we define as

$$\tilde{V}_{ij}^{(lm)}(kr) \equiv \int_0^{2\pi} \mathrm{d}\phi \int_0^{\pi} \mathrm{d}\vartheta \sin\vartheta \hat{e}_i^{(r)} V_j^{(lm)} \mathrm{e}^{-\mathrm{i}\boldsymbol{k}\boldsymbol{r}} \tag{21}$$

for the three cases $\boldsymbol{V}^{(lm)} = \{\boldsymbol{C}^{(lm)}, \boldsymbol{P}^{(lm)}, \boldsymbol{B}^{(lm)}\}$.

The displacement of the mode $\{nml\}$ induced by the force distribution $f_i^{(n)}(\boldsymbol{r}^{(0)})$ and the surface stresses $\sigma_{ij}^{(0)}(\boldsymbol{u})$ to a radially heterogeneous, anelastic self-gravitating Moon model can be derived from[1]

$$\begin{aligned} u_i^{(nml)}(\boldsymbol{r},t) = &\int_V \mathcal{G}_{ji}^{(nml)}(\boldsymbol{r}|\boldsymbol{r}^{(0)},t) f_j^{(n)}(\boldsymbol{r}^{(0)}) \mathrm{d}^3\boldsymbol{r}^{(0)} \\ &+ \int_S \mathcal{G}_{ji}^{(nml)}(\boldsymbol{r}|\boldsymbol{r}^{(0)},t) \hat{e}_k^{(r,0)} \sigma_{kj}^{(0)}(\boldsymbol{u}) \mathrm{d}S(\boldsymbol{r}^{(0)}) \end{aligned} \tag{22}$$

knowing the Green's function $\mathcal{G}^{(nml)}$. The Green's function

$$\mathcal{G}_{ij}^{(nml)}(\boldsymbol{r}|\boldsymbol{r}^{(0)},t) = Q_i^{*(nlm)}(\boldsymbol{r}) Q_j^{(nlm)}(\boldsymbol{r}^{(0)}) \bar{g}^{(n)}(t) (\Lambda_T^{(nml)})^{-1} \tag{23}$$

is in turn constructed out of the tensor product over the eigenvectors $Q_j^{(nlm)}$ for toroidal and spheroidal oscillations. Respectively, their normalizations are

$$\Lambda_T^{(nml)} = \frac{4\pi}{2l+1} l(l+1) \int_0^R [y_{1n}^T]^2 \rho^{(0)}(r) r^2 \mathrm{d}r, \tag{24}$$

$$\Lambda_S^{(nml)} = \frac{4\pi}{2l+1} \int_0^R ([y_{1n}^S]^2 + l(l+1)[y_{3n}^S]^2) \rho^{(0)}(r) r^2 \mathrm{d}r, \tag{25}$$

and the time dependence given by $\bar{g}(t)$. Inserting the driving force (5) and the surface stress (6) induced by a GW, we can rewrite Eq. (22) as

$$\begin{aligned} u_i^{(nml)}(\boldsymbol{r},t) = &-\int_V \frac{\mathrm{d}\mu}{\mathrm{d}r}(r) \mathcal{G}_{ij}^{(nml)}(\boldsymbol{r}|\boldsymbol{r}^{(0)},t) \hat{e}_k^{(r)} h^{kj} \mathrm{d}^3 r^{(0)} \\ &+ \mu(R) \int_S \mathcal{G}_{ij}^{(nml)}(\boldsymbol{r}|\boldsymbol{R},t) \hat{e}_k^{(r)} h^{kj} \mathrm{d}S^{(0)}(\boldsymbol{R}) \\ &- \frac{1}{2} \int_V \frac{\mathrm{d}\lambda}{\mathrm{d}r}(r) \mathcal{G}_{ij}^{(nml)}(\boldsymbol{r}|\boldsymbol{r}^{(0)},t) \hat{e}_j^{(r)} h \mathrm{d}^3 r^{(0)} \\ &+ \frac{1}{2} \lambda(R) \int_S \mathcal{G}_{ij}^{(nml)}(\boldsymbol{r}|\boldsymbol{R},t) \hat{e}_j^{(r)} h \mathrm{d}S^{(0)}(\boldsymbol{R}). \end{aligned} \tag{26}$$

To proceed, we have to distinguish between toroidal and spheroidal modes, using the results for the parameter functions y_i obtained in the Appendix. We will start with the simpler case of toroidal oscillations, checking explicitly that also the new contributions induced by the scalar polarization state in the GW are suppressed.

1. GW induced toroidal motion

In the toroidal case, we can simplify the displacement of the mode $\{nml\}$ using Eq. (A7) to

$$\boldsymbol{u}_j^{(nml)}(\boldsymbol{r},t) = l(l+1) h_0 \bar{g}(t) (\Lambda^{(nml)})^{-1} y_{1n}(r) C_j^{*(lm)}(\vartheta,\phi) F_T \tag{27}$$

with

$$\begin{aligned} F_T = &R^2 y_{1n}(R) \left[\mu(R)\mathcal{E}^{ij} + \frac{1}{2}\lambda(R)\delta_{ij}\right] \tilde{C}_{ij}^{(lm)}(kR) \\ &- \int_0^R \mathrm{d}r r^2 y_{1n}(r) \left[\frac{\mathrm{d}\mu(r)}{\mathrm{d}r}\mathcal{E}^{ij} + \frac{1}{2}\frac{\mathrm{d}\lambda(r)}{\mathrm{d}r}\delta_{ij}\right] \tilde{C}_{ij}^{(lm)}(kr), \end{aligned} \tag{28}$$

where we introduced the Fourier transform of the vector surface harmonics defined in Eq. (21).

Following Ben-Menahem [3], we take now advantage of the low-frequency limit: Since the fundamental frequency ν_1 of the Moon is in the mHz range, it holds that $c/2\pi\nu_1 \gg R$. This implies that the arguments kr and kR of the exponential functions in $\tilde{C}$ are slowly varying. Performing then a partial-wave expansion of $\tilde{C}$, only the partial waves with the lowest angular momentum have to be kept. We split the calculation into a μ and a λ dependent part; the latter is absent in Einstein gravity. In the Appendix, we elucidate the details of the partial-wave expansion of $\tilde{C}$, which results for the term including μ and its derivative in

[1]For a textbook discussion, see Ref. [3].

$$\frac{\sqrt{l(l+1)}}{8\pi \mathrm{i}} F_T^{(\mu)} = \mu(R) R^2 y_{1n}^T(R) \sum_{l_1=0}^{\infty} \sum_{m_l=-l_1}^{l_1} (2l_1+1) \mathrm{i}^{-l_1} j_{l_1}(kR) Y_{l_1}^{*m_1}(0,0) \begin{pmatrix} l_1 & l & 1 \\ 0 & 0 & 0 \end{pmatrix} \mathcal{E}^{ij} \sum_{k=-2}^{2} T_{ij}^{(k)} A^{(k)}$$
$$- \sum_{l_1=0}^{\infty} \sum_{m_l=-l_1}^{l_1} (2l_1+1) \mathrm{i}^{-l_1} Y_{l_1}^{*m_l}(0,0) \begin{pmatrix} l_1 & l & 1 \\ 0 & 0 & 0 \end{pmatrix} \mathcal{E}^{ij} \sum_{k=-2}^{2} T_{ij}^{(k)} A^{(k)} \int_0^R \frac{\mathrm{d}\mu}{\mathrm{d}r} y_{1n}^T(r) j_{l1}(kr) r^2 \mathrm{d}r, \quad (29)$$

where $T^{(k)}$ and $A^{(k)} = A^{(k)}(l_1, m_1, l, m)$ are given in the Appendix. The terms including λ and its derivative involve only the $A^{(0)}$ term and are given by

$$\frac{\sqrt{l(l+1)}}{4\pi} F_T^{(\lambda)} = \lambda(R) R^2 y_{1n}^T(R) \sum_{l_1=0}^{\infty} \sum_{m_l=-l_1}^{l_1} (2l_1+1) \mathrm{i}^{-l_1} j_{l_1}(kR) Y_{l_1}^{*m_1}(e,\lambda) \begin{pmatrix} l_1 & l & 1 \\ 0 & 0 & 0 \end{pmatrix} A^{(0)}$$
$$+ \sum_{l_1=0}^{\infty} \sum_{m_l=-l_1}^{l_1} (2l_1+1) \mathrm{i}^{-l_1} Y_{l_1}^{*m_l}(e,\lambda) \begin{pmatrix} l_1 & l & 1 \\ 0 & 0 & 0 \end{pmatrix} A^{(0)} \int_0^R \frac{\mathrm{d}\lambda}{\mathrm{d}r} y_{1n}^T(r) j_{l1}(kr) r^2 \mathrm{d}r. \quad (30)$$

For the case of $F_T^{(\lambda)}$, the mode of particular interest is the case $l = m = 2$, as it is the lowest mode capable of oscillations. Taking the sum over l_1, we observe that $A^{(0)}$ vanishes for all l_1. Therefore, we need to consider only $F_T^{(\mu)}$. In F_T, we have introduced Wigner's $6j$ symbols $\begin{pmatrix} a & b & c \\ c & d & e \end{pmatrix}$ which are defined in Eq. (B1). Assuming a spherical body, we are free to rotate the coordinate system in such a way to align the momentum vector of the gravitational wave with the z axis of our coordinate system, $k_i = \omega \hat{e}_i^{(z)}$. The choice of coordinate system is also the reason for why $Y_{l_1}^{*m_1}(\psi, \chi)$ which depends in general on the angles of the incoming GW wave simplifies to $Y_{l_1}^{*m_1}(0,0)$ in (29). The contraction of the polarization tensor with the T matrix given in the Appendix results in

$$\mathcal{E}_{ij} \sum_{k=-2}^{2} T^{ij(k)} A^{(k)} = \frac{\mathrm{i}}{2\sqrt{2}} \sqrt{(l+m)(l-m+1)} \times \begin{pmatrix} l_1 & l & 1 \\ m_1 & m-1 & -1 \end{pmatrix}. \quad (31)$$

Since the Bessel function $j_l(x)$ satisfies

$$j_l(x) \simeq \frac{1}{(2l+1)!!} (x)^l \quad (32)$$

for $x \to 0$, we have a series which very quickly converges given that $x \ll 1$. Inserting for (32) and (31) in (29) gives

$$\frac{\sqrt{l(l+1)}}{8\pi \mathrm{i}} F_T^{(\mu)} = \sum_{l_1=0}^{\infty} \sum_{m_l=-l_1}^{l_1} \mathrm{i}^{-l_1} \frac{(2l_1+1)}{(2l_1+1)!!} \sqrt{(l+m)(l-m+1)} \sqrt{\frac{(l_1-m_1)!}{(l_1+m_1)!}} P_{l_1}^{m_1}(1) \begin{pmatrix} l_1 & l & 1 \\ 0 & 0 & 0 \end{pmatrix} \begin{pmatrix} l_1 & l & 1 \\ m_1 & m-1 & -1 \end{pmatrix}$$
$$\times \left[\mu(R) R^2 y_{1n}^T(R) (kR)^{l_1} - \int_0^R \frac{\mathrm{d}\mu}{\mathrm{d}r} y_{1n}^T(r) (kr)^{l_1} r^2 \mathrm{d}r \right]. \quad (33a)$$

Together with the time dependence (11b) and the normalization (24), we now have all the required ingredients to calculate the toroidal displacement after having determined numerically the parameter function $y_{1n}(r)$.

2. GW induced spheroidal motion

Following the same strategy as in the toroidal case, we obtain using (A13) for the induced displacement in the case of spheroidal oscillations

$$u_j^{(nml)}(\boldsymbol{r}, t) = h_0 \bar{g}(t) (\Lambda_S^{nml})^{-1} \left[P_j^{*(nml)}(\boldsymbol{r}) F_{S_1} + l(l+1) B_j^{*(nml)}(\boldsymbol{r}) F_{S_2} \right], \quad (34)$$

where F_{S_1} and F_{S_2} are given by

$$\sqrt{l(l+1)} F_{S_1} = R^2 \mu(R) y_{1n}(R) \mathcal{E}^{ij} \tilde{P}_{ij}^{(lm)}(kR) - \int_0^R \frac{\mathrm{d}\mu}{\mathrm{d}r} y_{1n}(r) r^2 dr \mathcal{E}^{ij} \tilde{P}_{ij}^{(lm)}(kr), \quad (35)$$

$$\sqrt{l(l+1)}F_{S_2} = R^2\mu(R)y_{1n}(R)\mathcal{E}^{ij}\tilde{B}^{(lm)}_{ij}(kR) - \int_0^R \frac{\mathrm{d}\mu}{\mathrm{d}r} y_{1n}(r) r^2 dr \mathcal{E}^{ij}\tilde{B}^{(lm)}_{ij}(kr). \quad (36)$$

Note that the terms including the first Lamé parameter λ do not contribute to spheroidal oscillations; see the Appendix for further details. In order to simplify the expressions for F_{S_1} and F_{S_2}, we will study the (reducible) quadrupole moment D_{ij} of the Moon,

$$\mathcal{D}_{ij} = 3\int_V r_i r_j \rho \mathrm{d}V. \quad (37)$$

Here, we kept the trace $\mathcal{D}_{ii}$ which can couple to the scalar polarization state of the GW. For a displacement $r_i \to r_i + u_i$, the change of quadrupole moment to first order is

$$\delta\mathcal{D}_{ij} = 3\int_V (r_i u_j + u_i r_j)\rho \mathrm{d}V. \quad (38)$$

If we consider only a single spheroidal mode, then we can represent the displacement contribution to $\delta\mathcal{D}_{\mu\nu}$ by

$$u^{(nml)}_j = y_{1n}P^{ml}_j + y_{3n}\sqrt{l(l+1)}B^{ml}_j. \quad (39)$$

Inserting (39) into (38), we can split the total quadruple moment into

$$\delta\mathcal{D}^{(P)}_{ij} = 3\int_0^R y_{1n}(r)\rho^{(0)}(r)r^2\mathrm{d}r(\tilde{P}^{(ml)}_{ij}(r) + \tilde{P}^{(ml)}_{ji}(r)), \quad (40a)$$

$$\delta\mathcal{D}^{(B)}_{ij} = 3\sqrt{l(l+1)}\int_0^R y_{3n}(r)\rho^{(0)}(r)r^2\mathrm{d}r(\tilde{B}^{(ml)}_{ij}(r) + \tilde{B}^{(ml)}_{ji}(r)). \quad (40b)$$

Neglecting the phase factor, we can express F_{S_1} and F_{S_2} via the changes of the quadruple moment as

$$F_{S_1} = \frac{R^2\mu(R)y_{1n}(R) - \int_0^R \dot{\mu}y_{1n}(r)r^2\mathrm{d}r}{3\int_0^R \rho_0 y_{1n}(r)r^2\mathrm{d}r}\mathcal{E}^{ij}\delta\mathcal{D}^{(P)}_{ij}, \quad (41)$$

$$F_{S_2} = \frac{R^2\mu(R)y_{3n}(R) - \int_0^R \dot{\mu}y_{3n}(r)r^2\mathrm{d}r}{3\int_0^R \rho_0 y_{3n}(r)r^2\mathrm{d}r}\mathcal{E}^{ij}\delta\mathcal{D}^{(B)}_{ij}. \quad (42)$$

Thus, these functions are proportional to the interaction between the GW and the reducible quadrupole moment of the spherical body.

We employ as in the toroidal case the low-frequency approximation. Starting from Eqs. (B18) and (B22) for the Fourier transformed surface harmonics derived in the Appendix, we consider the limit $kr \to 0$. Then, the Bessel function simplifies to $j_{l_1}(0) = \delta_{l_1,0}$. Forcing $l_1 = 0$ for a nonzero result puts strict restrictions on the Wigner symbols in $D^{(j)}$, and the integrals simplify to

$$\tilde{P}^{(lm)}_{ij}(0) = \frac{4\pi}{5}\delta_{l,2}(\Gamma^{(0)}_{ij}\delta_{m,0} - \Gamma^{(1)}_{ij}\delta_{m,-1} + \Gamma^{(-1)}_{ij}\delta_{m,1} + \Gamma^{(2)}_{ij}\delta_{m,-2} + \Gamma^{(-2)}_{ij}\delta_{m,2}), \quad (43a)$$

$$\sqrt{l(l+1)}\tilde{B}^{(lm)}_{ij}(0) = \frac{12\pi}{5}\delta_{l,2}(\Gamma^{(0)}_{ij}\delta_{m,0} - \Gamma^{(1)}_{ij}\delta_{m,-1} + \Gamma^{(-1)}_{ij}\delta_{m,1} + \Gamma^{(2)}_{ij}\delta_{m,-2} + \Gamma^{(-2)}_{ij}\delta_{m,2}). \quad (43b)$$

If we insert this into the equations (40) for the change in the quadrupole moment, we obtain

$$\delta\mathcal{D}_P + \delta\mathcal{D}_B = \frac{24\pi}{5\sqrt{6}}\delta_{l,2}\Delta\int_0^R (y_{1n} + 3y_{3n})\rho_0(r)r^2\mathrm{d}r \quad (44)$$

with

$$\Delta = \begin{pmatrix} \delta_{m,2} + \delta_{m,-2} - \sqrt{\frac{2}{3}}\delta_{m,0} & \mathrm{i}\delta_{m,2} - \mathrm{i}\delta_{m,-2} & \delta_{m,1} + \delta_{m,-1} \\ \mathrm{i}\delta_{m,2} - \mathrm{i}\delta_{m,-2} & -\delta_{m,2} - \delta_{m,-2} - \sqrt{\frac{2}{3}}\delta_{m,0} & -\mathrm{i}\delta_{m,-1} + \mathrm{i}\delta_{m,1} \\ \delta_{m,1} + \delta_{m,-1} & -\mathrm{i}\delta_{m,-1} + \mathrm{i}\delta_{m,1} & 2\sqrt{\frac{2}{3}}\delta_{m,0} \end{pmatrix}.$$

The quadrupole tensor has to be contracted with the polarization tensor of the GW. Because of the Kronecker delta $\delta_{l,2}$, only spheroidal oscillations with $l = 2$ will contribute in this approximation. The contribution of the scalar polarization state is given by

$$h_s\left(\delta_{m,2} + \delta_{m,-2} - \sqrt{\frac{2}{3}}\delta_{m,0}\right) + h_s\left(-\delta_{m,2} - \delta_{m,-2} - \sqrt{\frac{2}{3}}\delta_{m,0}\right) = -2h_s\sqrt{\frac{2}{3}}, \quad (45)$$

while the standard TT polarizations from Einstein gravity result in

$$2h_+(\delta_{m,2}+\delta_{m,-2}) \quad \text{and} \quad 2ih_\times(\delta_{m,2}-\delta_{m,-2}). \tag{46}$$

D. Numerical determination of $y_i(r)$

The last ingredient needed to calculate the displacement of the Moon surface are the parameter functions $y_{1n}(r)$. For their numerical determination, we follow the procedure described in Chap. 6.7 of Ref. [3]. In the toroidal case, we impose the boundary conditions (A11) on the system of differential equations (A12). A guess for y_1 at the core-mantle boundary $r=a$ and for the eigenfrequency ω is used to begin the integration. The eigenfrequency is then adjusted after the integration until the second boundary condition for y_2 is satisfied. Lastly, y_1 is normalized. In the spheroidal case, the numerical procedure for solving the system of differential equation system is more complicated, since we have to consider also the liquid core. The integration is therefore split into two systems: One differential equation system for the core (A27) and one system for the mantle (A25). More specifically, two initial conditions are chosen for y_2 and y_6 at $r=0$, while the remaining initial conditions are set to zero. We use a Runge-Kutta solver to integrate the system (A27) over the core. The end values are used as initial values for the second integration over the mantle, except for y_3, where the initial condition is chosen similarly to y_2 and y_6 at the start. Integration is then done from $r=a$ to $r=R$. We perform this integration three times with differently chosen initial conditions for y_2, y_6, and y_3. Then, we construct the matrix

$$\begin{bmatrix} y_2^{(1)} & y_2^{(2)} & y_2^{(3)} \\ y_4^{(1)} & y_4^{(2)} & y_4^{(3)} \\ y_6^{(1)}+\frac{l(l+1)}{R}y_5^{(1)} & y_6^{(2)}+\frac{l(l+1)}{R}y_5^{(2)} & y_6^{(3)}+\frac{l(l+1)}{R}y_5^{(3)} \end{bmatrix}_{r=R}.$$

The eigenfrequency is varied until the determinant of the matrix changes sign. The zero determinant of the matrix signals that all boundary conditions are satisfied and the eigenfrequency is found.

In order to test our numerical procedure, we applied it to the Jeffreys-Bullen A' model and found good agreement with the eigenfrequencies and y_i functions described in Ref. [21]; for more details on the numerical implementation and the tests, see Ref. [22].

IV. LUNAR RESPONSE TO GRAVITATIONAL WAVES

A. Moon models

We use the three different models for the interior of the Moon presented in Ref. [23] to analyze its response to GWs. The key characteristics of each model, the density $\rho(r)$, the Lamé parameters $\lambda(r)$ and $\mu(r)$, and the gravitational acceleration $g(r)$, are shown in Fig. 1. The three models agree well with each other in most of the mantle, while in the core, deviations are stronger. Moreover, the models slightly disagree on the value of the core radius a. The deviations are largest for the first Lamé parameter $\lambda(r)$ in the core.

B. Eigenfrequencies and displacement

1. Eigenfrequencies and normal modes

The first four eigenfrequencies $\nu_i=\omega_i/2\pi$ of the three models are shown in Table I, for toroidal oscillations on the top and spheroidal oscillations on the bottom. The fundamental eigenfrequencies of all three models agree very well, with deviations in the pro mille range, despite rather large model differences especially in the core. The variation of the eigenfrequencies between the three models increases with n, reaching already 20% for $n=4$. Similarly, the differences in the eigenfrequencies between toroidal and spheroidal oscillations are small for $n=1$, and increase with n.

In the case of spheroidal oscillations ${}_mS_l$, the leading contribution in the long-wavelength limit $kr\to 0$ is given by $l_1=0$. Taking into account the condition (43) in Eq. (44), we have seen that then only $l=\pm 2$ modes contribute to spheroidal oscillations. Thus, we have to consider only the ${}_2S_2$ mode for the cross- and plus polarization, and the ${}_0S_2$ mode for the scalar polarization state. In the case of toroidal oscillations, the $l_1=0$ term vanishes, and the leading contribution is thus given by $l_1=1$. In this case, we have to consider only the ${}_2T_2$ mode for the possible three polarization states of the GW.

2. Displacement

Since the perturbations of a spherically symmetric body factorize in an angular and a radial dependent part, it is useful to split the displacement into a part characterizing the overall magnitude of the mode,

$$\xi_T(t)=h_0(\Lambda_T^{022})^{-1}F_T\bar{g}(t), \tag{47}$$

$$\xi_S(t)=h_0(\Lambda_S^{022})^{-1}(F_{S_1}+F_{S_2})\bar{g}(t), \tag{48}$$

neglecting the angular-dependent modulation determined by the $\tilde{V}$ functions. For the time dependence $\bar{g}_n(t)$, we use Eq. (13) where we assume as quality factor $Q_1=3300$ for the first eigenfrequency for all Moon models, following Ref. [23]. Moreover, we consider first the displacement of the models at resonance, i.e., when $\omega_0=\omega_1$, where ω_0 is the frequency of the GW.

We begin with the toroidal response. In Fig. 2, we show the toroidal displacement ξ_T for the ${}_2T_2$ mode using the Moon model 1 and setting $h_0=1$. Moreover, we have here assumed $A_+=A_\times=1$. The shape of the oscillation pattern

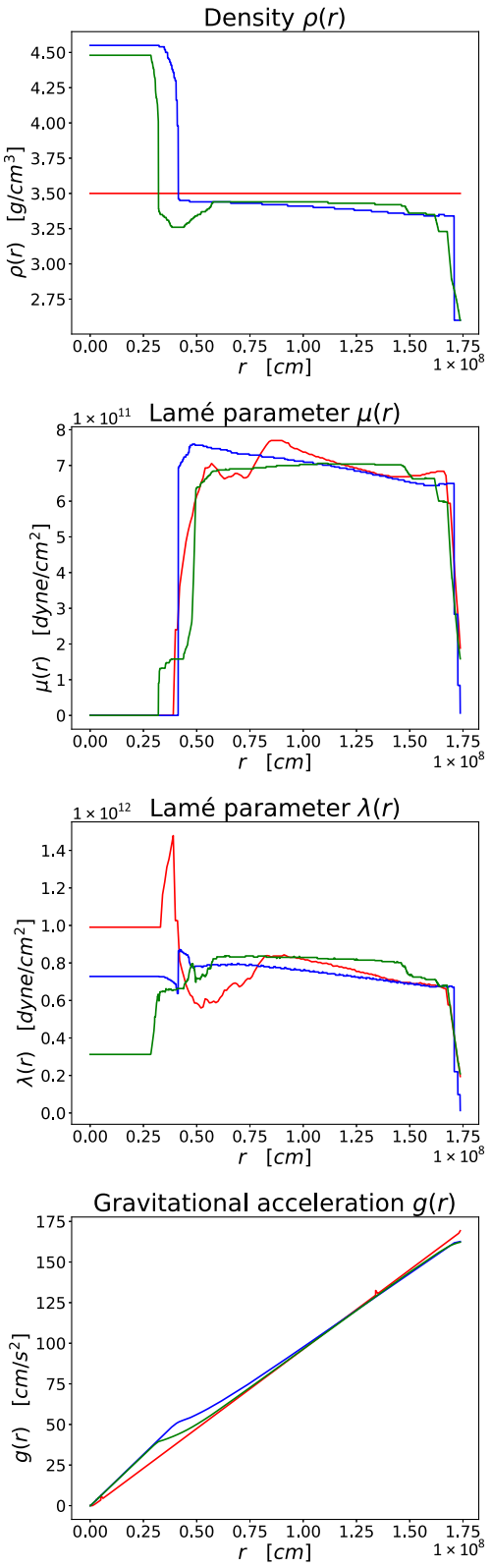

FIG. 1. The parameters $\rho(r)$, $\mu(r)$, $\lambda(r)$, and $g(r)$ of the three Moon models. Model 1 in red, model 2 in blue, and model 3 in green.

TABLE I. The first four toroidal (top) and spheroidal (bottom) eigenfrequencies ν_i in ms^{-1} of the three Moon models.

n	Model 1	Model 2	Model 3
1	0.993	1.014	1.011
2	2.901	2.950	2.918
3	4.266	4.388	4.079
4	5.635	5.869	4.929
1	1.020	1.050	1.047
2	1.848	1.890	1.892
3	2.932	2.881	2.686
4	3.976	3.993	3.412

is independent of the specific model, and only the magnitude ξ_T varies. The values of ξ_T determined by our numerical integrations are summarized in Table II. The toroidal displacement of the Moon is typically 2 orders of magnitude larger than for the Earth. There is only a minor difference between model 1 and 3, while the response in model 2 is a factor 5 smaller. Looking back at Fig. 1, we do observe that model 2 differs from the other two models

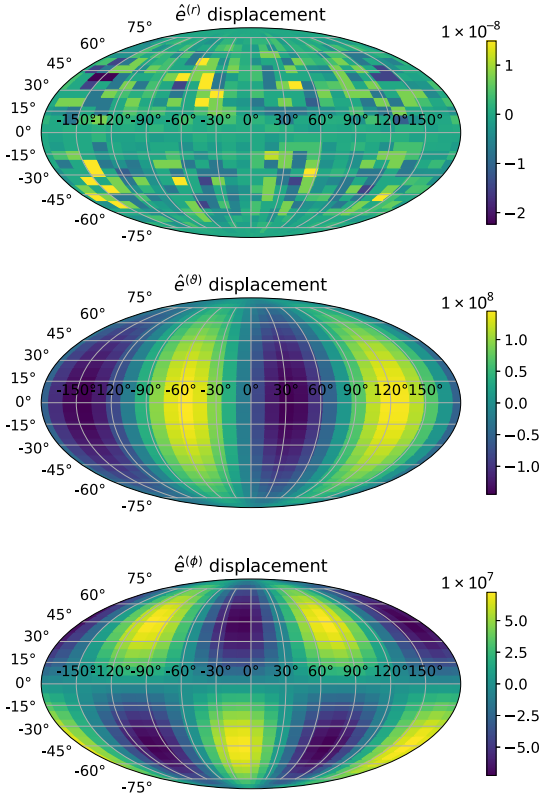

FIG. 2. The ${}_2T_2$ displacement per unit strain $h_0 = 1$ of Moon model 1 to a plus and cross-polarized GW in units of cm. The top figure is the displacement in the $\hat{e}^{(r)}$ direction, the middle figure is in the $\hat{e}^{(\vartheta)}$ direction, and the bottom figure is in the $\hat{e}^{(\phi)}$ direction.

TABLE II. The displacement ξ_T/h_0 and ξ_S/h_0 for the different Moon models and the ${}_2T_2$, ${}_2S_2$, and ${}_0S_2$ mode for $\omega_0 = \omega_1$.

Mode	Model 1	Model 2	Model 3
${}_2T_2$	4.478×10^7 cm	9.612×10^7 cm	4.722×10^7 cm
${}_2S_2$	1.288×10^{13} cm	1.900×10^{13} cm	3.636×10^{12} cm
${}_0S_2$	1.051×10^{13} cm	1.549×10^{13} cm	2.969×10^{12} cm

close to the surface, particularly in the second Lamé parameter $\mu(r)$: This parameter is in model 2 two orders lower than in models 1 and 3.

We proceed to the displacement from the spheroidal oscillations. In Fig. 3, we show the displacement for the ${}_2S_2$ mode in model 1. Comparing the values for ξ_S given for the three Moon models in Table II, we do observe the opposite trend as for the toroidal mode in that the response of model 2 is larger than in the other models. Also, the three models agree better than in the toroidal case. This different behavior may arise from the spheroidal response depending also on the parameter values of the core and not just the mantle as in the toroidal case.

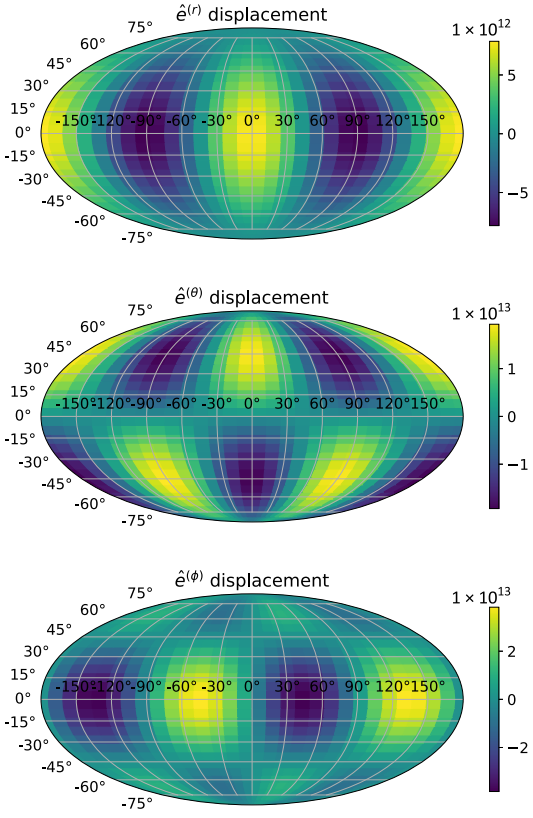

FIG. 3. The ${}_2S_2$ displacement of Moon model 1 to a plus- and cross-polarized gravitational wave in units of cm. The top figure shows the displacement in the $\hat{e}^{(r)}$ direction, the middle figure shows the displacement in the $\hat{e}^{(\vartheta)}$ direction, and the bottom figure shows the displacement in the $\hat{e}^{(\phi)}$ direction.

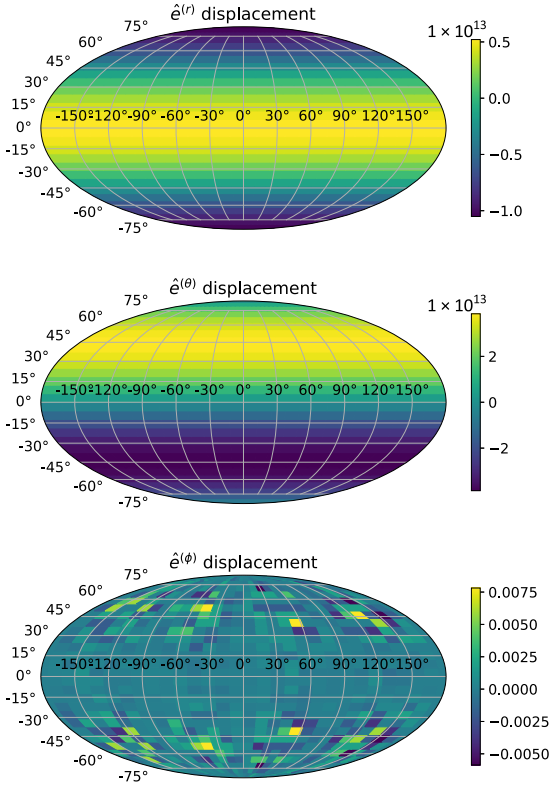

FIG. 4. The ${}_0S_2$ displacement of Moon model 1 to a scalar polarized gravitational wave in cm. The top model shows the displacement in the $\hat{e}^{(r)}$ direction, the middle model shows the displacement in the $\hat{e}^{(\vartheta)}$ direction, and the bottom model shows the displacement in the $\hat{e}^{(\phi)}$ direction.

The last mode for discussion is the mode excited by the scalar polarized gravitational wave ${}_0S_2$. The response for the first model is plotted in spherical coordinates in Fig. 4. The values of ξ_S follow a similar pattern, with the largest response in model 2, while the weakest response happens in model 1. For all models, the response to the scalar mode ${}_0S_2$ is smaller than for the ${}_2S_2$ modes. The ratio of the displacement for ${}_0S_2$ and ${}_2S_2$ modes is in agreement with the factor $\sqrt{2/3}$ difference found in Eqs. (45) and (46).

In addition to the resonance case, we report in Table III the response at a frequency in between the two first eigenfrequencies, which we choose as $\omega_0 = (\omega_1 + \omega_2)/2$. At such an intermediate frequency, where the response

TABLE III. The displacement ξ_T/h_0 and ξ_S/h_0 for the different Moon models and the ${}_2T_2$, ${}_2S_2$, and ${}_0S_2$ mode for $\omega_0 = (\omega_1 + \omega_2)/2$,.

Mode	Model 1	Model 2	Model 3
${}_2T_2$	0.803×10^4 cm	1.774×10^4 cm	0.857×10^4 cm
${}_2S_2$	3.529×10^{10} cm	4.574×10^{10} cm	3.369×10^{10} cm
${}_0S_2$	2.881×10^{10} cm	3.735×10^{10} cm	2.751×10^{10} cm

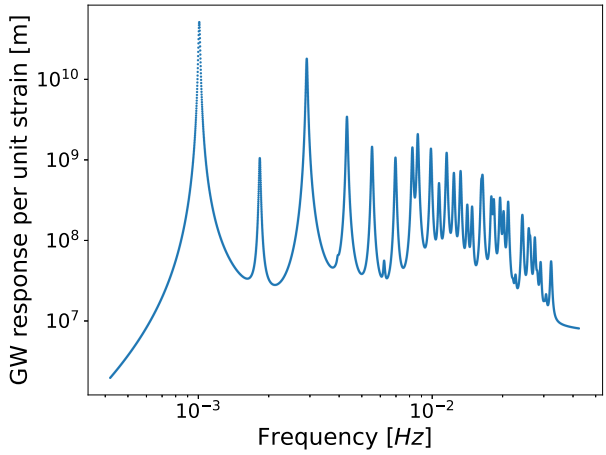

FIG. 5. The gravitational wave response in Moon model 1 including the first 37 eigenfrequencies with $Q_n = \text{const}$ using the response function given in Eq. (13).

should be less dependent on the specific choice of the Green's function $G_n(\omega)$, the response is reduced, which can also be seen clearly from Fig. 5.

We can make a crude estimate of the magnitude of the scalar amplitude expected for the GW signal from a Galactic neutron star. Following Ref. [24], the amplitude of a plus-polarized gravitational wave from a slightly perturbed rotating neutron star can be expressed as

$$h_+(t) = \frac{16\pi^2 G}{c^4}(1-\zeta)Q\frac{f_0^2}{r}\cos 2\phi(t), \tag{49}$$

where ζ is the Brans-Dicke parameter, Q is the quadrupol moment, and f_0 and ϕ are the rotational frequency and angle of the star. Still following Ref. [24], the scalar polarization can be expressed as

$$h_s(t) = -\frac{4\pi G}{c^3}\zeta\left(D\frac{f_0}{r}\sin\phi(t) - \frac{4\pi}{c}Q\frac{f_0^2}{r}\cos 2\phi(t)\right) \tag{50}$$

with D as the stellar dipole moment. Choosing $\phi(t) = \pi/2$, we obtain as estimate for the ratio of the scalar and plus-polarized response

$$\frac{h_s}{h_+} = -\frac{\zeta}{1-\zeta}\left(\frac{c}{4\pi f_0}\frac{D}{Q} + 1\right). \tag{51}$$

Reference [25] reports the bound $\zeta < 1.25 \times 10^{-5}$. We can make a crude estimate of the ratio h_s/h_+ by considering $f_0 = 100$ Hz and $Q = 10^{33}$ kg m^2. Moreover, we choose $D = 10^{29}$ kg m and $D = 0$ to bracket the range for the stellar dipole moment. With these values, we arrive at the following estimates,

$$\frac{h_s}{h_+} \lesssim 3 \times 10^{-4} \quad \text{and} \quad \frac{h_s}{h_+} \lesssim 1 \times 10^{-5}, \tag{52}$$

for a nonzero and zero dipole moment, respectively.

3. Total response over frequency

We have up to this point kept our focus mainly on the first eigenfrequency of the Moon models, having presented the response of the Moon only for this frequency. Since the frequency of the GW will in general not match the eigenfrequency of the Moon, or may cover a broad range of frequencies, it is necessary to study how the response changes as we move to other frequencies for the incoming GW. If we again assume a GW with the momentum vector $\boldsymbol{k} = (0, 0, \omega_0)$, then the expression for the main contribution from spheroidal oscillations is

$$u_i^{(nml)}(\boldsymbol{r}, t) = h_0(\Lambda^{(nml)})^{-1}\bar{g}(t)Q_i^{*(nml)}(\boldsymbol{r})(F_{S_1} + F_{S_2}). \tag{53}$$

We set now $h_0 = 1$, considering the response per unit strain, and neglect the angular dependence as well, defining $\xi^{nml}(t) = (\Lambda^{(nml)})^{-1}\bar{g}(t)(F_{S_1} + F_{S_2})$. We are interested in the total response, and we must therefore sum over eigenfrequencies. We restrict the analysis to the $l = 2$ and $m = 2$ modes,

$$\xi_{\text{tot}}(t) = \sum_{n=1}^{\infty}\xi^{n22}(t). \tag{54}$$

We choose the time t such that the response is maximal and assume that the response from all the eigenfrequencies adds constructively. Moreover, we consider as a signal a finite monochromatic wave with duration $\tau = T_1$, where $T_1 = 2\pi/\omega_1$ is the eigenperiod of the first eigenfrequency.

We show the gravitational response per unit strain as a function of the frequency of the incoming GW in Fig. 5. We choose again as quality factor $Q_0 = 3300$ for the first eigenfrequency. The frequency dependence of the quality factors Q_n for higher eigenmodes of the Moon is rather uncertain: The authors of Ref. [26] found $Q_n \propto \omega^{0.7}$ in the range 3–8 Hz for S waves, while for P waves, no significant frequency dependence was found. As there are no determinations of the frequency dependence of Q in the most interesting range mHz–Hz range, we choose Q_n as a constant, $Q_n = Q_0 = 3300$.

We observe a general trend of decreasing response at higher resonances, its degree being dependent on the frequency dependence of the quality factor Q_n. At the same time, the distance between resonance frequencies decreases as we move to higher frequencies in Fig. 5, indicating that the Moon becomes a broadband detector for $\omega \gg \omega_1$. At frequencies smaller than the first eigenfrequency, we observe a strong suppression of the response. This implies that the detectability of GWs with frequencies less than mHz is unlikely.

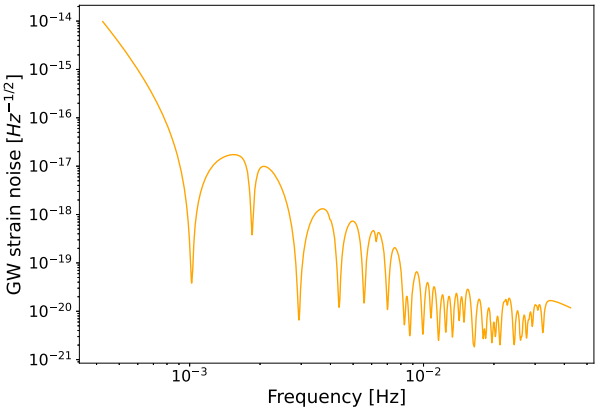

FIG. 6. Sensitivity of the LGWA experiment for the most recent detector concept [19] as function of frequency ν with $Q_n = \text{const}$ using the response function given in Eq. (13).

We can summarize our results in the sensitivity plot shown in Fig. 6. Using the minimal acceleration predicted for two different detector concepts proposed for the LGWA experiment, we show the detection capabilities of the proposed LGWA experiment for ${}_2S_2$ modes in the Moon model 1. Using the values from Table II, the sensitivity curves for other models can be obtained performing a simple overall shift of the curves for model 1.

Finally, we want to compare our results with earlier ones, in particular with those shown by the LGWA Collaboration in Fig. 1 from Ref. [11]. In order to compare more easily to our results we choose now the same quality factor of $Q_n = 200$ for all eigenfrequencies. Moreover, we use now instead of Eq. (13) the Green's function employed in Ref. [11],

$$\bar{g}(t) = \frac{1}{\omega_n^2 - \omega_0^2 + \mathrm{i}\omega_n^2/Q_n}. \tag{55}$$

The resulting gravitational response per unit strain as a function of the frequency of the incoming GW is shown in Fig. 7. Compared to Fig. 1 Ref. [11], we note that the positions of the first resonance as well as the overall shape agree well, while the asymptotic value for large frequencies in our case is a factor of a few higher.

Note that, while the response for our default Green's function is real, we have to take the real part of the complex response obtained using Eq. (55). Consequently, the strain in Fig. 7 oscillates around the asymptotic value, while the strain in Fig. 5 approaches the asymptotic value from above. Taking into account this difference, our results for the two different Green's functions agree for large frequencies (and the same value for the quality factor Q_n). On the other hand, the larger value of quality factor $Q_n = 3300$ used by us in the main part of our analysis explains the larger sensitivities found by us. This difference in the used quality factor explains also the difference in the overall scale seen in the sensitivity plot 7, while the variation in shape is caused by the differences in the Green's function used. In addition, we show in Fig. 8 the expected sensitivity

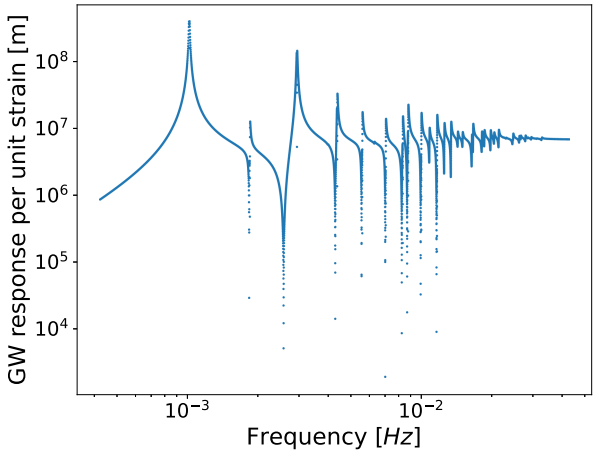

FIG. 7. The gravitational wave response in Moon model 1 including the first 37 eigenfrequencies with $Q_n = \text{const}$ using the response function given in Eq. (55).

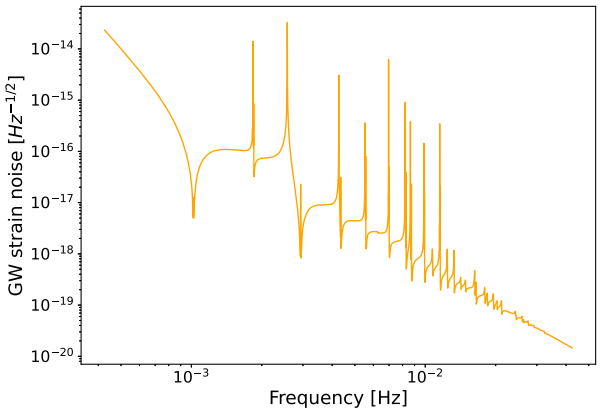

FIG. 8. Sensitivity of the LGWA experiment for the most recent detector concept [19] as function of frequency ν with $Q_n = \text{const}$ using the response function given in Eq. (55).

of the LGWA experiment using the response function given in Eq. (55). This sensitivity curve can be compared to the one shown in Fig. 3, which shows qualitatively a similar behavior.

V. CONCLUSIONS

We have studied the response of the Moon to gravitational perturbations in general scalar-tensor theories of gravity. Our semianalytic study was based on the approach developed by Alterman *et al.* [4] for the study of seismic waves in the Earth. Its main limitation is the restriction to heterogeneous but spherically symmetric Moon models.

We have analyzed three sets of Moon models which are based on different methodologies to determine the Moon interior. The variation of these models is largest in the first Lamé parameter λ which determines the response to bulk forces and therefore does not contribute to spheroidal oscillations. As a result, the displacement and the

eigenfrequencies of the first eigenmodes determined by us numerically agree relatively well for the three different Moon models; the variations between the different models are, however, increasing for larger n. Using the reach in measuring accelerations predicted for the LGWA experiment from Ref. [11], we found a nominal sensitivity of this experiment to GWs with amplitude $h \simeq 10^{-20}$ for quality factors $Q_n \simeq 3300$ in the mHz range.

ACKNOWLEDGMENTS

This work was motivated by the presentations at the "Lunar session" of the 2022 Vulcano Workshop "Frontier Objects in Astrophysics and Particle Physics." We would like to thank the organizers and participants, and in particular the late Stavros Katsanevas, for raising our interest in this topic. We are grateful to Jan Harms for useful comments on the manuscript and the LGWA experiment.

APPENDIX A: REDUCTION TO FIRST-ORDER EQUATIONS

In this Appendix, we will transform the Euler and Poisson equation to a system of first-order equations, which is more suitable both for numerical integration and for imposing the appropriate boundary conditions, following the approach of Ref. [21].

1. Boundary conditions

We have to impose the following four boundary conditions:

(1) The solution is well defined at the origin.
(2) The stresses vanish at the deformed surfaces and stay continuous at an internal deformed surface of discontinuity.
(3) The displacements are continuous at an internal surface of discontinuity, with the exception of a solid-liquid interface where only the radial displacement is continuous.
(4) The gravitational potential and its radial derivative are continuous at the deformed surface of the Earth at an internal deformed surface of discontinuity.

In order to implement these boundary conditions mathematically, we consider the stresses close to a surface of discontinuity at $r = c$ in a strained state,

$$\begin{aligned}\sigma_{jk}(c+u_r) &= \sigma_{jk}(c) + u_r\left(\frac{\partial \sigma_{jk}}{\partial r}\right)_{r=c} \\ &= \sigma^{(e)}_{jk}(c) - P^{(0)}(c)\delta_{jk}. \end{aligned} \tag{A1}$$

The additional elastic stresses at c and at $c + u_r$ are equal to first order in u_r. We also see that a small element of the medium carries its initial stress with it when it moves from one place to another. The boundary condition 4 regards only the gravitational potential. Mathematically, it says that

$$\Psi_< = \Psi_> \quad \text{and} \quad \frac{\mathrm{d}\Psi_<}{\mathrm{d}r} = \frac{\mathrm{d}\Psi_>}{\mathrm{d}r} \quad \text{at } r = c + u_r, \tag{A2}$$

where the indices $<$ and $>$ indicate that Ψ and Ψ' are evaluated at opposite sides of the surface of discontinuity. Expanding Ψ around its equilibrium value and using the Poisson equation, it follows that

$$\frac{\mathrm{d}^2\Psi^{(0)}}{\mathrm{d}r^2} + \frac{2}{r}\frac{\mathrm{d}\Psi^{(0)}}{\mathrm{d}r} = -4\pi G\rho^{(0)} \tag{A3}$$

and

$$\psi_< = \psi_>, \quad \dot{\psi}_< - 4\pi G\rho^{(0)}_< u_r = \dot{\psi}_> - 4\pi G\rho^{(0)}_> u_r. \tag{A4}$$

At the surface of the Moon, we then must have that

$$\psi = \psi^{(e)}, \qquad \dot{\psi} - 4\pi G\rho^{(0)} u_r = \dot{\psi}^{(e)}, \tag{A5}$$

where ψ_e is the gravitational potential outside the spherical model.

2. Toroidal oscillations

For purely toroidal oscillations, u_r and $u_{j,j}$ both vanish. The Euler equation (19) then simplifies to

$$\mu\Delta u_j + \frac{\mathrm{d}\mu}{\mathrm{d}r}\left(2\frac{\partial u_j}{\partial r} + \epsilon_{jab}\hat{e}^{(r)}_a \epsilon_{bcd}\nabla_c u_d\right) + \omega^2\rho^{(0)}u_j = 0. \tag{A6}$$

Setting $U^{(n)} = V^{(n)} = 0$ in Eq. (9) appropriate for toroidal oscillations, we can write the displacement as

$$\begin{aligned} u_j(\boldsymbol{r}) &= \sum_{\sigma,m,l} Q_j^{(nml)}(\boldsymbol{r}) \\ &= \sum_{\sigma,m,l} y_1(r)\sqrt{l(l+1)}C_j^{(\sigma ml)}(\vartheta,\phi), \quad \sigma = c,s. \end{aligned} \tag{A7}$$

Here, we have split the displacement into a sum over the core and mantle contributions, $\sigma = \{c, s\}$, to make sure that the solution is well defined at both the origin and in all parts of the mantle. We insert our ansatz into (19) and arrive at a new differential equation for y_1,

$$\begin{aligned} &\mu\left(\frac{\mathrm{d}^2 y_1}{\mathrm{d}r^2} + \frac{2}{r}\frac{\mathrm{d}y_1}{\mathrm{d}r}\right) + \frac{\mathrm{d}\mu}{\mathrm{d}r}\left(\frac{\mathrm{d}y_1}{\mathrm{d}r} - \frac{y_1}{r}\right) + \omega^2\rho^{(0)}y_1 \\ &\quad - \frac{l(l+1)}{r^2}\mu y_1 = 0. \end{aligned} \tag{A8}$$

By boundary condition 2, we must have that the stresses vanish at the core-mantle boundary. We therefore define a function y_2 such that this function is zero at the boundary. We write the stress in the radial direction and define y_2 as

$$\hat{e}_i^{(r)}\sigma_{ij} = \sum_{\sigma,m,l} y_2(r)\sqrt{l(l+1)}\boldsymbol{C}_j^{(\sigma ml)}(\vartheta,\phi), \quad \sigma = c,s. \tag{A9}$$

We find y_2 more explicitly inserting Eq. (A7) into $\sigma_{ij}(\boldsymbol{u})$,

$$y_2 = \mu\left(\frac{dy_1}{dr} - \frac{y_1}{r}\right). \tag{A10}$$

Boundary condition 2 requires then the following conditions on y_2,

$$y_2 = 0 \quad \text{at } r = r_c \quad \text{and} \quad r = R. \tag{A11}$$

In order to avoid numerical problems caused by the derivative $\mathrm{d}\mu/\mathrm{d}r$ in Eq. (A8), it is more convenient to use the equivalent system of differential equations

$$\frac{\mathrm{d}y_1}{\mathrm{d}r} = \frac{y_1}{r} + \frac{y_2}{\mu}, \tag{A12a}$$

$$\frac{\mathrm{d}y_2}{\mathrm{d}r} = \left(\frac{l^2+l-2}{r^2}\mu - \omega^2\rho^{(0)}\right)y_1 - \frac{3}{r}y_2. \tag{A12b}$$

3. Spheroidal oscillations

Spheroidal oscillations were defined as displacements involving the vector surface harmonics $\boldsymbol{P}$ and $\boldsymbol{B}$ only. Thus, a spheroidal displacement can be written as

$$\begin{aligned} u_j(\boldsymbol{r}) &= \sum_{\sigma,m,l} Q_j^{(nml)}(\boldsymbol{r}) \\ &= \sum_{\sigma,m,l}\big(y_{1n}(r)P_j^{(\sigma ml)}(\vartheta,\phi) \\ &\quad + y_{3n}(r)\sqrt{l(l+1)}B_j^{(\sigma ml)}(\vartheta,\phi)\big). \end{aligned} \tag{A13}$$

We decompose the gravitational perturbation as

$$\psi(\boldsymbol{r}) = \sum_{\sigma,m,l} y_{5n}(r)Y_l^{(\sigma)m}(\vartheta,\phi). \tag{A14}$$

Inserting Eqs. (22) and (A14) into the Euler and Poisson equations results in a system of differential equations for y_1, y_3, and y_5. A lengthy, but not too complicated, calculation of inserting Eq. (22) into (19) and setting the coefficients of $P_i^{(ml)}$ and $B_i^{(ml)}$ to zero leads to the system

$$\mu\left(2\frac{\mathrm{d}X}{\mathrm{d}r} - \frac{l(l+1)}{r}Z\right) + \frac{\mathrm{d}(\lambda X)}{\mathrm{d}r} + 2\dot{\mu}\frac{\mathrm{d}y_1}{\mathrm{d}r} + \rho^{(0)}\left[\frac{\mathrm{d}y_5}{\mathrm{d}r} - 4\pi G\rho^{(0)}y_1 + g^{(0)}\left(X - \frac{\mathrm{d}y_1}{\mathrm{d}r} + \frac{2}{r}y_1 + \omega^2 y_1\right)\right] = 0, \tag{A15}$$

$$(\lambda+2\mu)\frac{X}{r} - \frac{\mathrm{d}}{\mathrm{d}r}(\mu Z) - \mu\frac{Z}{r} + 2\dot{\mu}\left(\frac{\mathrm{d}y_3}{\mathrm{d}r} + Z\right) + \rho_0\left(\frac{1}{r}(y_5 - g^{(0)}y_1) + \omega^2 y_3\right) = 0 \tag{A16}$$

with

$$\begin{aligned} X &= \frac{\mathrm{d}y_1}{\mathrm{d}r} + \frac{2}{r}y_1 - \frac{l(l+1)}{r}y_3, \\ \text{and} \quad Z &= \frac{1}{r}(y_1 - y_3) - \frac{\mathrm{d}y_3}{\mathrm{d}r}. \end{aligned} \tag{A17}$$

To accommodate the boundary conditions and to obtain a system of first-order differential equations, we evaluate the elastic stress. Setting

$$\begin{aligned} \hat{e}_i^{(r)}\sigma_{(e)}^{ij} &= \sum_{\sigma,m,l}\big(y_2(r)P_j^{(\sigma ml)}(\vartheta,\phi) \\ &\quad + y_4(r)\sqrt{l(l+1)}B_j^{(\sigma ml)}(\vartheta,\phi)\big), \end{aligned} \tag{A18}$$

we find y_2 and y_4 as

$$y_2 = \lambda X + 2\mu\frac{\mathrm{d}y_1}{\mathrm{d}r} = (\lambda+2\mu)\frac{\mathrm{d}y_1}{\mathrm{d}r} + \frac{2\lambda}{r}y_1 - \lambda\frac{l(l+1)}{r}y_3, \tag{A19}$$

$$y_4 = \mu\left(Z + 2\frac{\mathrm{d}y_3}{\mathrm{d}r}\right) = \mu\left(\frac{1}{r}(y_1 - y_3) + \frac{\mathrm{d}y_3}{\mathrm{d}r}\right). \tag{A20}$$

We now insert (A14) into (20) to obtain a differential equation for y_5,

$$\frac{\mathrm{d}^2y_5}{\mathrm{d}r^2} + \frac{2}{r}\frac{\mathrm{d}y_5}{\mathrm{d}r} - \frac{l(l+1)}{r^2}y_5 = 4\pi G(\rho^{(0)}X + \dot{\rho}^{(0)}y_1). \tag{A21}$$

With $\Delta\psi_e = 0$ outside the boundary of the spherical model, the boundary condition becomes

$$\frac{\mathrm{d}y_5}{\mathrm{d}r} - 4\pi G\rho^{(0)}y_1 = -\frac{l+1}{r}y_5 \quad \text{at } r = R. \tag{A22}$$

Defining a new function y_6 as

$$y_6 = \frac{\mathrm{d}y_5}{\mathrm{d}r} - 4\pi G\rho^{(0)}y_1, \tag{A23}$$

the boundary conditions at $r = R$ become

$$y_2 = 0, \qquad y_4 = 0, \qquad y_6 + \frac{l+1}{r} y_5 = 0. \tag{A24}$$

We now treat $y_1, y_2, \ldots, y_6$ as independent variables, obtaining a system of first-order differential equations valid in the mantle,

$$\frac{\mathrm{d}y_1}{\mathrm{d}r} = -\frac{2\lambda}{(\lambda+2\mu)r} y_1 + \frac{1}{\lambda+2\mu} y_2 + \frac{l(l+1)\lambda}{(\lambda+2\mu)r} y_3, \tag{A25a}$$

$$\frac{\mathrm{d}y_2}{\mathrm{d}r} = \left[-\omega^2 \rho^{(0)} - 4\frac{g^{(0)}\rho_0}{r} + \frac{4\mu(3\lambda+2\mu)}{(\lambda+2\mu)r^2}\right] y_1 - \frac{4\mu}{(\lambda+2\mu)r} y_2 + \frac{l(l+1)}{r}\left[g^{(0)}\rho^{(0)} - \frac{2\mu(3\lambda+2\mu)}{(\lambda+2\mu)r}\right] y_3 + \frac{l(l+1)}{r} y_4 - \rho^{(0)} y_6 \tag{A25b}$$

$$\frac{\mathrm{d}y_3}{\mathrm{d}r} = -\frac{1}{r} y_1 + \frac{1}{r} y_3 + \frac{1}{\mu} y_4 \tag{A25c}$$

$$\frac{\mathrm{d}y_4}{\mathrm{d}r} = \left[\frac{g^{(0)}\rho^{(0)}}{r} - \frac{2\mu(3\lambda+2\mu)}{(\lambda+2\mu)r^2}\right] y_1 - \frac{\lambda}{(\lambda+2\mu)r} y_2 \tag{A25d}$$

$$+\left(-\omega^2\rho^{(0)} + ((2l^2+2l-1)\lambda + 2(l^2+l-1)\mu)\frac{2\mu}{(\lambda+2\mu)r^2}\right) y_3 - \frac{3}{r} y_4 - \frac{\rho_0}{r} y_5 \tag{A25e}$$

$$\frac{\mathrm{d}y_5}{\mathrm{d}r} = 4\pi G \rho^{(0)} y_1 + y_6, \tag{A25f}$$

$$\frac{\mathrm{d}y_6}{\mathrm{d}r} = -4\pi \frac{l(l+1)}{r} G\rho^{(0)} y_3 + \frac{l(l+1)}{r^2} y_5 - \frac{2}{r} y_6. \tag{A25g}$$

In the core, on the other hand, we have

$$\mu = 0, \qquad y_2 = \lambda X, \qquad y_4 = 0, \tag{A26}$$

resulting in a simpler system of differential equations,

$$\frac{\mathrm{d}y_1}{\mathrm{d}r} = -\frac{2}{r} y_1 + \frac{1}{\lambda} y_2 + \frac{l(l+1)}{r} y_3, \tag{A27a}$$

$$\frac{\mathrm{d}y_2}{\mathrm{d}r} = -\left(\omega^2\rho^{(0)} + \frac{4g^{(0)}\rho^{(0)}}{r}\right) y_1 + \frac{l(l+1)}{r} g^{(0)}\rho^{(0)} y_3 - \rho^{(0)} y_6, \tag{A27b}$$

$$\frac{\mathrm{d}y_5}{\mathrm{d}r} = 4\pi G\rho^{(0)} y_1 + y_6 \tag{A27c}$$

$$\frac{\mathrm{d}y_6}{\mathrm{d}r} = -4\pi \frac{l(l+1)}{r} G\rho^{(0)} y_3 + \frac{l(l+1)}{r^2} y_5 - \frac{2}{r} y_6. \tag{A27d}$$

The parameter function y_4 is zero in the core. We find an expression for y_3 using (A25e) and (A26),

$$y_3 = \frac{1}{\omega^2 r}\left(g_0 y_1 - \frac{1}{\rho_0} y_2 - y_5\right). \tag{A28}$$

APPENDIX B: EXPANSION OF THE FOURIER TRANSFORMS $\tilde{V}_{ij}^{(lm)}$

In this Appendix, we will express the Fourier transforms $\tilde{V}_{ij}^{(lm)}(x)$ of the three vector surface harmonics in terms of spherical Bessel functions $j_l(x)$ with Wigner's $6j$ symbols as expansion coefficients. For the later, we use the following convention:

$$\begin{pmatrix} l_1 & l_2 & l_3 \\ m_1 & m_2 & m_3 \end{pmatrix} = W \sum_n \frac{(-1)^{l_1-l_2-m_3+n}}{n!} \left(\frac{\Pi_{i=1}^3 (l_i+m_i)!(l_i-m_i)!}{(l_1+l_2-l_3-n)!(l_1-m_1-n)!(l_2+m_2-n)!} \right) \times (l_3-l_2+m_1+n)!(l_3-l_1-m_2+n)!, \tag{B1}$$

with

$$W = \sqrt{\left(\frac{\Pi_{i=1}^3 (2p-2l_i)!}{(2p+1)!} \right)} \delta_{m_1+m_2-m_3} \tag{B2}$$

and $2p = l_1 + l_2 + l_3$. The sum goes over positive values of n until the denominator of the expression becomes negative. The symbols are nonzero only, when

$$m_1 + m_2 + m_3 = 0, \quad \text{and} \quad |l_a - l_b| \le l_c \le |l_a + l_b|, \tag{B3}$$

with $a, b, c = \{1, 2, 3\}$. These two relations allow one to quickly determine if the Wigner symbols are zero.

Our aim is to evaluate the Fourier transforms $V_{ij}^{(ml)}(kr)$ defined by Eq. (21) for the three cases $\boldsymbol{V}^{(ml)} = \{\boldsymbol{C}^{(ml)}, \boldsymbol{P}^{(ml)}, \boldsymbol{B}^{(ml)}\}$. We begin with the $\boldsymbol{C}$ function, writing it in spherical coordinates,

$$\sqrt{l(l+1)} C_j^{(ml)} = \left(\hat{e}_j^{(\vartheta)} \frac{1}{\sin\vartheta} \partial_\phi - \hat{e}_j^{(\phi)} \partial_\vartheta \right) Y_{(l)}^{(m)}. \tag{B4}$$

In order to unclutter the notation, we will omit the parentheses around m and l in the spherical harmonics Y_l^m, which we define as

$$Y_l^m(\vartheta, \phi) = \sqrt{\frac{(l-m)!}{(l+m)!}} P_l^m(\cos\vartheta) e^{im\phi}. \tag{B5}$$

We can write this vector in Cartesian components as

$$\sqrt{l(l+1)} C_j^{(ml)} = a_j^{(0)} Y_l^m + a_j^{(+)} Y_l^{m+1} + a_j^{(-)} Y_l^{m-1}, \tag{B6}$$

where $a_j^{(0)}$, $a_j^{(+)}$, and $a_j^{(-)}$ are combinations of the Cartesian unit vectors given by

$$a_j^{(0)} = -im \hat{e}_j^{(z)}, \tag{B7}$$

$$a_j^{(\pm)} = \frac{i}{2} \sqrt{(l \mp m)(l \pm m + 1)} (\hat{e}_j^{(x)} \mp i \hat{e}_j^{(y)}). \tag{B8}$$

Assuming a general momentum vector,

$$k_i = \omega(\sin\psi\cos\chi, \sin\psi\sin\chi, \cos\psi), \tag{B9}$$

we perform next a partial-wave expansion of the exponential,

$$e^{-i\boldsymbol{k}\boldsymbol{r}} = \sum_{l_1=0}^{\infty} \sum_{m_1=-l_1}^{l_1} (2l_1+1) i^{-l_1} j_{l_1}(kr) Y_{l_1}^{m_1}(\vartheta, \phi) Y_{l_1}^{*m_1}(\psi, \chi), \tag{B10}$$

and inserting (B6) and (B10) into $\tilde{C}_{ij}^{(lm)}(kr)$, we obtain

$$\begin{aligned} &\sqrt{l(l+1)} \tilde{C}_{jk}^{(ml)}(kr) \\ &= \sum_{l_1=0}^{\infty} \sum_{m_1=-l_1}^{l_1} (2l_1+1) i^{-l_1} j_{l_1}(kr) \\ &\quad \times Y_{l_1}^{*m_1}(\psi, \chi) (A_j^{(0)} a_k^{(0)} + A_j^{(+)} a_k^{(+)} + A_j^{(-)} a_k^{(-)}) \end{aligned} \tag{B11}$$

with

$$A_j^{(n)} = \int_0^{2\pi} \int_0^{\pi} \hat{e}_\alpha^{(r)} Y_{l_1}^{*m_1}(\vartheta, \phi) Y_l^{m+n}(\psi, \chi) \sin\vartheta d\vartheta d\phi. \tag{B12}$$

Using the identity

$$\begin{aligned} &\int_0^{2\pi} d\phi \int_0^{\pi} d\vartheta \sin\vartheta Y_{l_1}^{m_1} Y_{l_2}^{m_2} Y_{l_3}^{m_3} \\ &\quad = 4\pi \begin{pmatrix} l_1 & l_2 & l_3 \\ 0 & 0 & 0 \end{pmatrix} \begin{pmatrix} l_1 & l_2 & l_3 \\ m_1 & m_2 & m_3 \end{pmatrix} \end{aligned} \tag{B13}$$

in (B11), we arrive at the result

$$\begin{aligned} \sqrt{l(l+1)} \tilde{C}_{jk}^{(ml)} &= 4\pi \sum_{l_1=0}^{\infty} \sum_{m_1=-l_1}^{l_1} (2l_1+1) i^{-l_1} j_{l_1}(kr) \\ &\quad \times Y_{l_1}^{*m_1}(\psi, \chi) \begin{pmatrix} l_1 & l_2 & 1 \\ 0 & 0 & 0 \end{pmatrix} \sum_{k=-2}^{2} A^{(k)} T^{(k)} \end{aligned} \tag{B14}$$

with

$$T^{(0)} = \begin{pmatrix} 0 & 0 & 0 \\ 0 & 0 & 0 \\ 0 & 0 & i \end{pmatrix}, \quad T^{(\pm 1)} = \frac{1}{2} \begin{pmatrix} 0 & 0 & \mp i \\ 0 & 0 & 1 \\ \mp i & 1 & 0 \end{pmatrix},$$
$$T^{(\pm 2)} = \mp \begin{pmatrix} \mp i & 1 & 0 \\ 1 & \pm i & 0 \\ 0 & 0 & 0 \end{pmatrix}, \tag{B15}$$

and

$$A^{(0)} = -m\begin{pmatrix} l_1 & l & 1 \\ m_1 & m & 0 \end{pmatrix} - \frac{1}{2\sqrt{2}}\sqrt{(l+m)(l-m+1)}\begin{pmatrix} l_1 & l & 1 \\ m_1 & m-1 & 1 \end{pmatrix} \tag{B16a}$$

$$+\frac{1}{2\sqrt{2}}\sqrt{(l-m)(l+m+1)}\begin{pmatrix} l_1 & l & 1 \\ m_1 & m+1 & -1 \end{pmatrix}, \tag{B16b}$$

$$A^{(\pm 1)} = -\sqrt{2}m\begin{pmatrix} l_1 & l & 1 \\ m_1 & m\mp 1 & \mp 1 \end{pmatrix} \mp \sqrt{(l\pm m)(l\mp m+1)}\begin{pmatrix} l_1 & l & 1 \\ m_1 & m\mp 1 & 0 \end{pmatrix}, \tag{B16c}$$

$$A^{(\pm 2)} = \frac{1}{2\sqrt{2}}\sqrt{(l\pm m)(l\mp m+1)}\begin{pmatrix} l_1 & l & 1 \\ m_1 & m\mp 1 & -1 \end{pmatrix}. \tag{B16d}$$

Next, we consider the case of the $\boldsymbol{P}$ integral. Using that in spherical coordinates $P_j^{(ml)} = \hat{e}_j^{(r)} Y_l^m(\vartheta,\phi)$, we apply again the partial-wave expansion (B10). The resulting product $\hat{e}_j^r \hat{e}_k^r$ can be written in terms of Cartesian unit coordinates and the associated Legendre polynomial as

$$\begin{aligned}\hat{e}_j^{(r)}\hat{e}_k^{(r)} = {} & \frac{1}{3}\delta_{jk} + \frac{1}{3}Y_2^0(\hat{e}_j^{(x)}\hat{e}_k^{(x)} - \hat{e}_j^{(y)}\hat{e}_k^{(y)} + 2\hat{e}_j^{(z)}\hat{e}_k^{(z)}) + \frac{1}{\sqrt{6}}Y_2^1(\hat{e}_j^{(z)}\hat{e}_k^{(-)} + \hat{e}_k^{(z)}\hat{e}_j^{(-)}) \\ & - \frac{1}{\sqrt{6}}Y_2^{-1}(\hat{e}_j^{(z)}\hat{e}_k^{(+)} + \hat{e}_k^{(z)}\hat{e}_j^{(+)}) + \frac{1}{\sqrt{6}}Y_2^2\hat{e}_j^{(-)}\hat{e}_k^{(-)} + \frac{1}{\sqrt{6}}Y_2^{-2}\hat{e}_j^{(+)}\hat{e}_k^{(+)},\end{aligned} \tag{B17}$$

where we have defined $\hat{e}^{(\pm)} = \hat{e}^{(x)} \pm \mathrm{i}\hat{e}^{(y)}$. Then, we employ the identity (B13) to obtain

$$\tilde{P}_{ij}^{(lm)}(kr) = 4\pi\sum_{l_1=0}^{\infty}\sum_{m_1=-l_1}^{l_1}(2l_1+1)\mathrm{i}^{-l_1}j_{l_1}(kr)Y_{l_1}^{*m_1}(\psi,\chi)\begin{pmatrix} l_1 & l & 2 \\ 0 & 0 & 0 \end{pmatrix}\sum_{j=-2}^{2}\Gamma_{ij}^{(j)}\begin{pmatrix} l_1 & l & 2 \\ m_1 & m & j \end{pmatrix}, \tag{B18}$$

where the $\Gamma^{(j)}$ symbols are defined as combinations of the Cartesian unit vectors,

$$\Gamma_{jk}^{(0)} = \frac{1}{3}(-\hat{e}_j^{(x)}\hat{e}_k^{(x)} - \hat{e}_j^{(y)}\hat{e}_k^{(y)} + 2\hat{e}_j^{(z)}\hat{e}_k^{(z)}), \qquad \Gamma_{jk}^{(\pm 1)} = \frac{1}{\sqrt{6}}(\hat{e}_j^{(z)}\hat{e}_k^{(\mp)} + \hat{e}_j^{(\mp)}\hat{e}_k^{(z)}), \qquad \Gamma_{jk}^{(\pm 2)} = \frac{1}{\sqrt{6}}\hat{e}_j^{(\mp)}\hat{e}_k^{(\mp)}. \tag{B19}$$

Finally, we have to evaluate the Fourier transform of the vector surface harmonics $\boldsymbol{B}$. Inserting into

$$\sqrt{l(l+1)}B_j^{(ml)} = \epsilon_{ikj}\hat{e}_i^{(r)}C_k^{(ml)} \tag{B20}$$

the expansion (B6) for $C_k^{(ml)}$, we obtain

$$\sqrt{l(l+1)}\hat{e}_i^{(r)}B_j^{(ml)} = \hat{e}_i^{(r)}(\epsilon_{abj}\hat{e}_a^{(r)}a_b^{(0)})Y_l^m + \hat{e}_i^{(r)}(\epsilon_{abj}\hat{e}_a^{(r)}a_b^{(+)})Y_l^{m+1} + \hat{e}_i^{(r)}(\epsilon_{abj}\hat{e}_a^{(r)}a_b^{(-)})Y_l^{m-1}. \tag{B21}$$

Next, we represent the products $\hat{e}_i^{(r)}\epsilon_{abj}\hat{e}_a^{(r)}a_b^{(0,\pm)}$ by the Γ symbols defined previously, dropping all antisymmetric parts, obtaining

$$\sqrt{l(l+1)}\tilde{B}_{jk}^{(ml)}(kr) = 4\pi\sum_{l_1=0}^{\infty}\sum_{m_1=-l_1}^{l_1}(2l_1+1)\mathrm{i}^{-l_1}j_{l_1}(kr)Y_{l_1}^{*m_1}(\psi,\chi)\begin{pmatrix} l_1 & l & 0 \\ 0 & 0 & 0 \end{pmatrix}\sum_{j=-2}^{2}D^{(j)}\Gamma_{ik}^{(j)}, \tag{B22}$$

where the $D^{(j)}$ are given by

$$D^{(0)} = -\frac{3}{2\sqrt{6}}\sqrt{(l-m)(l+m+1)}\begin{pmatrix} l_1 & l & 2 \\ m_1 & m+1 & -1 \end{pmatrix} - \frac{3}{2\sqrt{6}}\sqrt{(l+m)(l-m+1)}\begin{pmatrix} l_1 & l & 2 \\ m_1 & m-1 & 1 \end{pmatrix},$$

$$D^{(\pm 1)} = -\frac{m}{2}\begin{pmatrix} l_1 & l & 2 \\ m_1 & m & \pm 1 \end{pmatrix} - \frac{3}{2\sqrt{6}}\sqrt{(l\mp m)(l\pm m+1)}\begin{pmatrix} l_1 & l & 2 \\ m_1 & m\pm 1 & 0 \end{pmatrix} - \frac{1}{2}\sqrt{(l\pm m)(l\mp m+1)}\begin{pmatrix} l_1 & l & 2 \\ m_1 & m\mp 1 & \pm 2 \end{pmatrix},$$

$$D^{(\pm 2)} = \mp m\begin{pmatrix} l_1 & l & 2 \\ m_1 & m & \pm 2 \end{pmatrix} - \frac{1}{2}\sqrt{(l\mp m)(l\pm m+1)}\begin{pmatrix} l_1 & l & 2 \\ m_1 & m\pm 1 & \pm 1 \end{pmatrix}.$$

[1] J. Weber, Phys. Rev. **117**, 306 (1960).
[2] F. J. Dyson, Astrophys. J. **156**, 529 (1969).
[3] A. Ben-Menahem, Il Nuovo Cimento C **6**, 49 (1983).
[4] Z. Alterman, H. Jarosch, and C. L. Pekeris, Proc. R. Soc. A **252**, 80 (1959).
[5] R. A. Wiggins and F. Press, J. Geophys. Res. (1896-1977) **74**, 5351 (1969).
[6] T. S. Mast, J. E. Nelson, and J. A. Saarloos, Astrophys. J. Lett. **187**, L49 (1974).
[7] M. Coughlin and J. Harms, Phys. Rev. D **90**, 042005 (2014).
[8] J. Majstorović, S. Rosat, and Y. Rogister, Phys. Rev. D **100**, 044048 (2019); **103**, 029901(E) (2021).
[9] P. Amaro-Seoane, L. Bischof, J. J. Carter, M.-S. Hartig, and D. Wilken, Classical Quantum Gravity **38**, 125008 (2021).
[10] K. Jani and A. Loeb, J. Cosmol. Astropart. Phys. 06 (2021) 044.
[11] J. Harms *et al.* (LGWA Collaboration), Astrophys. J. **910**, 1 (2021).
[12] S. Katsanevas and P. Bernard, *Lunar Seismic and Gravitational Antenna, in Ideas for exploring the Moon with a large European lander* (ESA, Munich, 2020).
[13] P. Amaro-Seoane *et al.* (LISA Collaboration), arXiv:1702.00786.
[14] ET Steering Committee, Einstein Telescope design report update, available from European Gravitational Observatory, Document No. ET-0007B-20, 2020.
[15] W. L. James R. Bates and H. Kernaghan, *ALSEP Termination Report* (NASA Reference Publication 1036, Washington, DC, 1979).
[16] T. Kupfer, V. Korol, S. Shah, G. Nelemans, T. R. Marsh, G. Ramsay, P. J. Groot, D. T. H. Steeghs, and E. M. Rossi, Mon. Not. R. Astron. Soc. **480**, 302 (2018).
[17] P. Jordan, Z. Phys. **157**, 112 (1959).
[18] C. Brans and R. H. Dicke, Phys. Rev. **124**, 925 (1961).
[19] J. V. van Heijningen, H. J. M. ter Brake, O. Gerberding, S. Chalathadka Subrahmanya, J. Harms, X. Bian, A. Gatti, M. Zeoli, A. Bertolini, C. Collette *et al.*, J. Appl. Phys. **133**, 244501 (2023).
[20] E. Poisson and C. M. Will, *Gravity: Newtonian, Post-Newtonian, Relativistic* (Cambridge University Press, Cambridge, England, 2014).
[21] A. Ben-Menahem and S. J. Singh, *Seismic Waves and Sources* (Springer-Verlag, Berlin, Heidelberg, New York, 1981).
[22] M. P. Nödtvedt, Master's thesis, NTNU Trondheim, Trondheim, 2023, https://hdl.handle.net/11250/3080886.
[23] F. Garcia Raphael *et al.*, Space Sci. Rev. **215**, 50 (2019).
[24] P. Verma, Universe **7**, 235 (2021).
[25] C. M. Will, Living Rev. Relativity **17**, 4 (2014).
[26] Y. Nakamura and J. Koyama, J. Geophys. Res. **87**, 4855 (1982).